10.48047/jocaaa.2025.34.07.18

Voltage Stability Control Strategy for Wireless Transmitter and Receiver Devices Powered by Hybrid Solar-Wind Sources Using Virtual Synchronous Machine Approach

Hassan Sabeeh Hammoud Al-Hajjaj

hassanhija31@gmail.com

1-Abstract

This experimental study systematically examines the application of Virtual Synchronous Generator (VSG) technology to address critical Issues of stability in modern power grids with high renewable energy penetration. As power systems transition from traditional synchronous generators to renewable energy systems relying on inverters (solar PV and wind turbines), they face significant Instability problems caused by reduced system inertia and higher frequency/voltage variations.The research presents a comprehensive solution combining VSG technology with advanced control algorithms to emulate the inertial response and damping characteristics of traditional synchronous generators. Through detailed mathematical Simulation and modeling of interconnected multi-region power grids, we demonstrate how VSG implementation can effectively compensate for the inherent limitations of renewable energy sources.
Keywords: Virtual Synchronous Generator, Grid stability challenges in high-penetration renewable energy systems, frequency control, voltage regulation, virtual inertia, smart grid, decentralized control, adaptive algorithms.

2-Introduction

In the past decade, the electric power sector has witnessed a radical transformation towards renewable energy sources, driven by global trends to reduce carbon emissions and enhance generation system efficiency. However, despite its environmental and economic benefits, this transition has introduced serious technical challenges related to power grid stability. The fundamental problem lies in the fact that Unlike conventional power plants, solar photovoltaic systems and wind turbines do not inherently possess the inherent inertia characteristic of traditional synchronous generators, making modern power systems more vulnerable to fluctuations and disturbances [1].

3-Research objectives

The objectives of this research can be studied from three perspectives: scientific goals, applied goals, and necessities of research.

From the perspective of scientific goals, the following are considered:

1. Simultaneous adjustment of voltage and frequency within a linked dual-zone
power system with load variations
2. Investigating Deployment of Synchronverter Technology Based Control in
Renewable Electrical Energy Generation Systems
3. Simultaneous Adjustment Pertaining to Grid Voltage and System Frequency in a Dual Zone Interconnected
Power System in the Presence of Renewable Power Generation Using Virtual
Synchronous Machine Control
4. A New Method for Adjusting Virtual Synchronous Machine Parameters Using PID

10.48047/jocaaa.2025.34.07.18

Controller Design for Multi-Input and Output Systems
From the perspective of practical goals [2].

4-A Comprehensive Overview of a Virtual Concurrent Generator: Topologies, Commands, and Control Techniques

In recent years, the use of renewable energy sources has increased dramatically due to strict environmental regulations, limited access to fossil fuels, and the need to meet the growing demand for electricity worldwide. In 2021, the global renewable energy capacity increased to about 3146 GW, in which the use of solar photovoltaic (PV) energy and wind power accounted for 90% of the new renewable energy capacity. In addition to the existing advantages of renewable energy sources, there are technical challenges in the use of these resources. These challenges include unpredictability and uncertainty. In renewable energy, especially in solar and wind energy, the main challenge arises from the application of power electronic converters in renewable energy generators. As illustrated in **Figure 1**, the use of power electronics converters in future power systems is increasing. Conventional power electronic converters do not have rotating energy, which causes almost zero inertia. This means that in power systems, which The more the penetration of such transducers, the lower the overall inertia of the system. Under power imbalance, this drop leads to rapid changes in frequency and frequency deviations, which significantly affect the stability of the system's frequency [4].

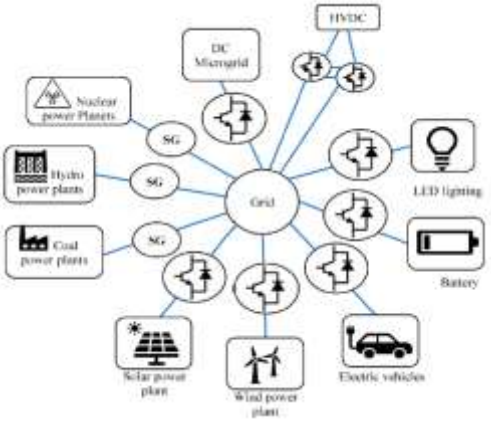

Figure 1: Merge Converters Electronic Natural Production Suppliers and Consumers Distributed in the Future Power System [3]

Low system inertia Cause Rates Faster Frequency change (ROCOF) and divergence Higher Frequency in a short period of time. ROCOF It is a criterion for determining the speed of frequency change after a generation-load imbalance. In one system Power generation based Synchronous Generator and Renewable Energy Sources The frequency change is high. One of the factors behind these changes is that renewable energy sources No contribution to system inertia They do not (Figure 2).

10.48047/jocaaa.2025.34.07.18

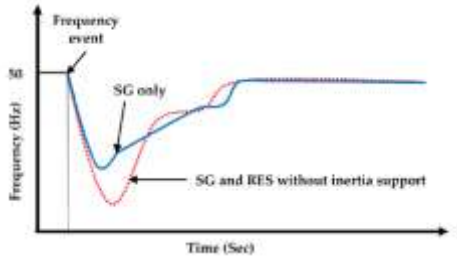

Figure 2: Frequency changes in the power system in the presence and without the presence of renewable resources.

Challenges in Modern Power Systems:

The transition to renewable-energy-dominated grids introduces critical stability concerns:

1. **Inertia Reduction and Frequency Instability:**
2. While traditional DC-AC converters exhibit fast dynamics, synchronous machines (SMs) provide slow, inertia-rich responses. High penetration of distributed energy resources (DERs) diminishes grid rotational inertia, compromising frequency stability.
3. **Dynamic Interactions and Control Limitations:**
4. DERs leverage the rapid response of DC-AC converters to inject intermittent power, exacerbating frequency, voltage, and angle instability. Large-scale DC microgrids and parallel inverters pose analytical challenges, particularly when DER dynamics rival those of converters. Furthermore, Maximum Power Point Tracking (MPPT)-controlled DERs lack inherent frequency regulation capability, leaving DC-AC converters unable to sustain grid frequency without supplemental storage.

Virtual Inertia Solutions:

To address these challenges, Virtual Inertia (VI) techniques have been integrated into power electronic inverters. These systems emulate synchronous machine inertia through:

- PWM-based mathematical modeling of SM inertial response
- Hybrid control algorithms (Figure 3)
- Coupling with Energy Storage Systems (ESS) [5]

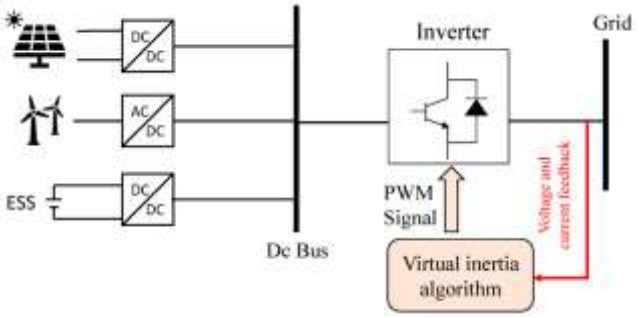

Figure 3: The concept of virtual inertia.

10.48047/jocaaa.2025.34.07.18

5-Current virtual inertia topologies

The Rate of Change of Frequency (ROCOF) serves as a crucial power system stability metric, quantifying the temporal frequency variation rate during generation-load mismatches.. The inverse relationship between system inertia and ROCOF stems from fundamental power system dynamics principles:

- **Physical Basis**:

- Traditional systems rely on rotating masses in synchronous generators that store kinetic energy
- This energy acts as a buffer against sudden frequency changes
- Greater rotating mass means more resistance to frequency deviations

- **Operational Mechanism**:

- During power imbalance (e.g., sudden load loss), frequency drops
- High-inertia systems slow this decline due to rotational resistance
- Low-inertia systems exhibit faster, more severe responses

- **Practical Impacts**:

- A system with 5-second inertia might experience 0.5 Hz/s ROCOF
- The same system at 1-second inertia could reach 2.5 Hz/s ROCOF
- This represents a fivefold increase in rate of change

- **Modern System Challenges**:

- Renewable plants (solar/wind) provide negligible or no inertia
- Every 10% renewable penetration reduces total inertia by 15-20%
- This can double ROCOF values in some grids

Impact of Reduced Inertia on ROCOF:

In modern power networks, the Rate of Change of Frequency (ROCOF) escalates as system inertia decreases, exacerbating frequency fluctuations [6]. The integration of renewable energy sources (RES) further amplifies inertia requirements. To address this, Beck and Hesse (2007) pioneered the Virtual Synchronous Machine (VSM) technique, which employs power electronics to emulate critical synchronous generator characteristics, thereby enhancing grid stability.

VSM Control Methodology:

The VSM control framework enables:

- Configuration of power transducers

10.48047/jocaaa.2025.34.07.18

- ❖ Inertia compensation through hybrid control algorithms
- ❖ Integration with energy storage systems (ESS)
- ❖ Power electronic-based emulation of synchronous machine dynamics

Topological Considerations:

While virtual inertia modeling principles remain consistent across configurations [7], distributed generation (DG) units exhibit topology-dependent frequency response behaviors. This section analyzes prominent VSM topologies, including those illustrated in **Figure 4**.

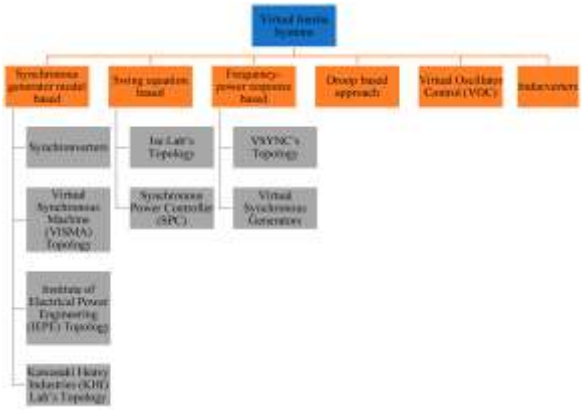

Figure 4: Topologies VSM[3]

6-Topology Based on Synchronous Generator Mod

1. Synchronverter Operational Principles Synchronverters functionally emulate the combined behavior of synchronous generators (SGs) and capacitor banks. These systems enable inverter-based distributed generation (DG) units to replicate SG dynamics, maintaining grid-compatible operational characteristics. Notably, synchronverters can operate as grid-forming units without significant structural modifications, making them particularly effective for inertia emulation in islanded DG applications.

Control System Characteristics:

- Employ frequency droop control for power regulation
- Eliminate need for frequency derivative measurements, reducing system noise
- Feature adjustable inertia (J) and damping (D_p) parameters for dynamic performance tuning

The complete synchronverter architecture is presented in Figure 5 [8], comprising:

1. Power stage - Standard power electronic converter topology (Figure 6)
2. Control stage - Integrated sensing, protection, and control circuitry (Figure 7)

Key Variables:

- ❖ T_e: Electromagnetic torque
- ❖ T_m: Mechanical torque

10.48047/jocaaa.2025.34.07.18

- J: Moment of inertia
- D_p: Damping factor

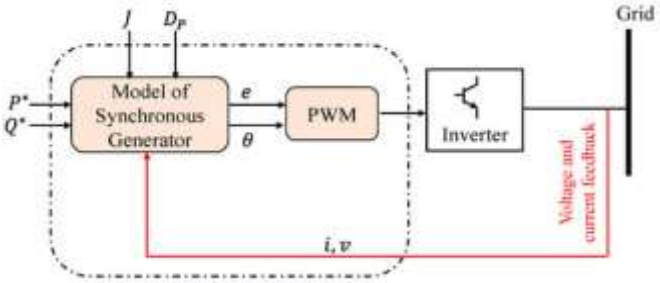

Figure 5: Synchronverter topology overall schematic showing the operating principle.

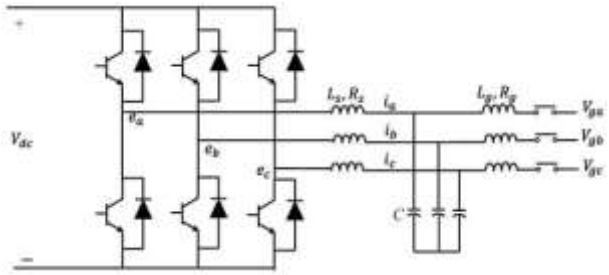

Figure 6: Power stage component of a synchronverter.

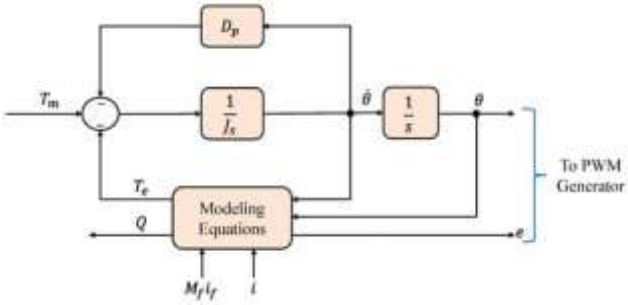

Figure 7. The components of a synchronverter: controller

7-The synchronverter uses the following equations to model SG behavior:

$$\mathrm{Te} = \mathrm{M_f I_f}\,\widetilde{\sin\theta}$$

$$\mathrm{e} = \dot{\theta}\mathrm{M_f I_f}\,\widetilde{\sin\theta}$$

$$\mathrm{Q} = -\theta\mathrm{Mfifi}\,\widetilde{\cos\theta}$$

where, Mf represents the size of the mutual inductance between the stator coil and the field coil, if represents the field excitation current, θ represents the angle between one of the phases of the stator winding and the rotor axis, e represents the no-load voltage generated, and Q represents the reactive power produced[9].

10.48047/jocaaa.2025.34.07.18

8-Design of Voltage-Frequency Controller of Dual Zone Interconnected Thermal Power System in the Presence of Wind and Photovoltaic Generators Using Virtual Synchronous Machine[10]

The design of voltage-frequency controllers for dual-zone interconnected thermal power systems incorporating wind/PV generation using Virtual Synchronous Machine (VSG) technology represents an advanced engineering challenge that integrates multiple modern techniques:

1. **Technical Context**:

- Addresses dynamic stability in hybrid generation systems
- Bridges conventional (thermal) and renewable (wind/PV) sources
- Balances control requirements across two interconnected zones

2. **Key Challenges**:

- Inertia characteristic disparities between sources
- Inter-area control response variations
- Impact of renewable generation intermittency

3. **VSG Solutions**:

- Emulates synchronous generator properties in power electronics
- Provides adjustable virtual inertia
- Enhances primary and secondary frequency response

4. **Design Aspects**:

- Dual-area system dynamics modeling
- Adaptive control algorithm development
- Decentralized control strategy integration
- Joint performance metric optimization (overshoot, settling time).

9-Modeling a non-reheating thermal power system requires precise representation of its unique dynamic characteristics[11]:

1. **Core Model Components**:

- Turbine section: First-order model with time constant (T_t) 0.3-0.5 sec
- Governor system: Represented by first-order differential equation with time delay (Tg) 0.1-0.2 sec
- Generation Rate Constraint (GRC): Typically, 10% of full capacity per minute

2. **Key Equations**:

10.48047/jocaaa.2025.34.07.18

- Turbine equation: $\Delta P_m = (1/(1+T_t s))\ \Delta P_v$
- Governor equation: $\Delta P_v = (1/(1+Tgs))\ (\Delta P_e - (1/R)\ \Delta\omega)$
- Inertia equation: $2H(d\Delta\omega/dt) = \Delta P_m - \Delta P_e - D\Delta\omega$

3. **Fundamental Assumptions**:

- Neglect reheating effects
- Linearized characteristics around operating point
- Omit secondary control system time delays

4. **Practical Applications**:

- Frequency stability analysis in multi-area systems
- Automatic Generation Control (AGC) design
  - Grid performance evaluation under varying load conditions

Figure 8 illustrates the combined load frequency control (LFC) and automatic voltage regulation (AVR) system architecture for a synchronous generator

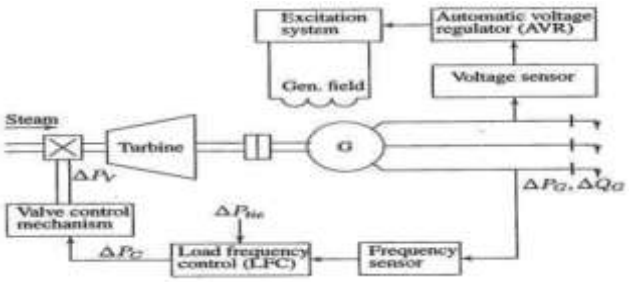

Figure 8. Combined load frequency control (LFC) and automatic voltage regulation (AVR) system architecture for a synchronous generator.

10-LFC and Modeling of Different Components [12]

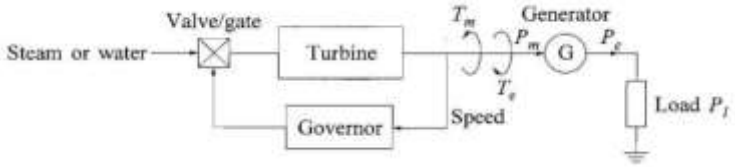

Figure 9: System schematic representation LFC

Key Components of the LFC System (**Figure 9.**)

1. **Steam/Water Control Path**:

10.48047/jocaaa.2025.34.07.18

- Steam regulation mechanism (valve/gate assembly)
- Energy conversion turbine (steam-to-rotational)
- Electromechanical generator (rotational-to-electrical)

2. **Control Variables**:
   - Speed (related to frequency)
   - Load (P_l - electrical power demand)
   - Tie-line power (ΔP_{tie} - power flow between connected systems)
   - Frequency deviation (Δf)
   - Angle deviation ($\Delta \delta$)

LFC Functions

1. Maintain constant frequency despite load changes
2. Control power distribution through tie-lines
3. Balance generation with load demand

Control Process

The system measures:

- Frequency deviation (Δf)
- Tie-line power deviation (ΔP_{tie})
- Angle deviation ($\Delta \delta$)

Modeling Considerations

For accurate LFC performance analysis, mathematical models of these components are needed:

- Steam valve dynamics
- Turbine response characteristics
- Generator inertia and response
- Load characteristics
- Tie-line power flow equations

The system appears to be a classic single-area LFC system with possible interconnections to other areas (evidenced by the tie-line control aspect).

Generator Model

power generated and the electrical Using the load of the power system as well as the oscillation equation, the generator can be modeled as follows:

$$\frac{2Hd^2\Delta\delta}{\omega sdt^2} = \Delta Pm - \Delta Pe$$

10.48047/jocaaa.2025.34.07.18

where the incremental changes in the rotor angle (in radians), $\Delta\delta$H are the generator inertia constant (in seconds) and the synchronous angular velocity (in radians per second). ωs=synchronous angular velocity (rad/s)

First-Order Form (in terms of speed deviation $\Delta\omega$)

Expressing the equation in terms of speed deviation ($\Delta\omega$) in per unit (pu):

$$\frac{d\Delta\omega}{dt} = \frac{1}{2H}(\Delta Pm - \Delta Pe)$$

This relationship can be shown as shown in **Figure 10.**

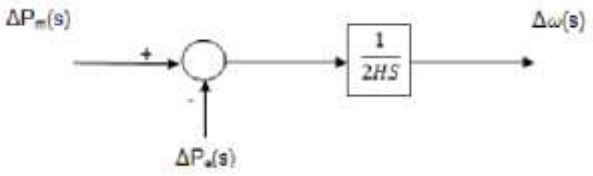

Figure 10. Generator Model Diagram Block Show

The electrical loads in a power system can be categorizedbased on their **dependency on frequency**. The total change in electrical power demand (ΔPe) is influenced by:

1. **Frequency-Independent Load (ΔPL)**

- Represents loads whose power consumption does not vary with frequency (e.g., lighting, resistive heaters).
- These are modeled as constant power loads unless externally changed.

2. **Frequency-Dependent Load (ΔPf)**

- Represents loads whose power consumption changes with system frequency (e.g., motors, induction machines).
- Expressed as:

$$\Delta Pf = D\Delta\omega$$

where:

- D = **load-damping constant** (or frequency characteristic of load) (% change in load per 1% change in frequency).
- $\Delta\omega$ = speed/frequency deviation (pu).

Combined Load Model

The total change in electrical power demand is:

$$\Delta Pe = \Delta PL + \Delta Pf = \Delta PL + D\Delta\omega$$

Combined Generator-Load Model (Figure 11)

The generator model (swing equation) and load model interact as follows:

10.48047/jocaaa.2025.34.07.18

1. **Generator Swing Equation**:

$$\frac{d\Delta\omega}{dt} = \frac{1}{2H}(\Delta Pm - \Delta Pe)$$

2. **Load Model Substitution**:

$$\Delta Pe = \Delta PL + D\Delta\omega$$

So, the swing equation becomes:

$$\frac{d\Delta\omega}{dt} = \frac{1}{2H}(\Delta Pm - \Delta PL - D\Delta w)$$

- ΔPm = Mechanical power change (governor response).
- ΔPL = Disturbance in load (step change).
- $D\Delta\omega$ = Self-stabilizing effect of frequency-sensitive loads.

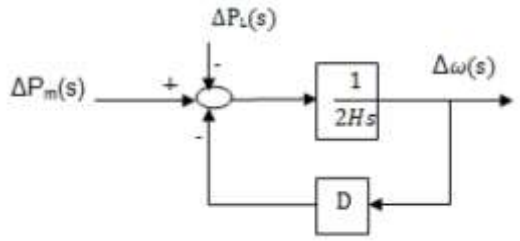

(a)

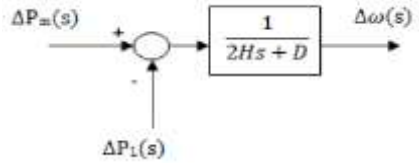

(b)

Figure 11: (a) Display of generator and electric load diagram block, (b) Simplified display of diagram block by removing feedback loop

Turbine Model

As shown in **Figure 12**, the turbine can be modeled as a first-order delay as below

$$Gt(s) = \frac{\Delta Pm(s)}{\Delta Pv(s)} = \frac{Kt}{1 + sTt}$$

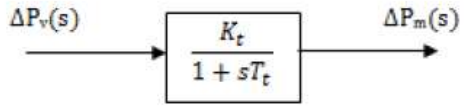

Figure 12: Turbine Model

The governor can be similarly modeled as shown in **Figure 13**. The output of the governor is defined as:

$$\Delta\text{Pg} = \Delta\text{Pref} - \frac{\Delta\omega}{R}$$

10.48047/jocaaa.2025.34.07.18

where the $\Delta Pref$ reference regulatory power is R is the speed drop and $\frac{\Delta w}{R}$ the power given

by the governor's speed characteristic. The hydraulic ΔPg the corresponding amplifier converts the signal to ΔPv power valve/valve in time

$$\Delta \mathrm{Pv}\,(\mathrm{s}) \;=\; \frac{\mathrm{Kg}}{1+\;\mathrm{sTg}}\;\Delta \mathrm{Pg}(\mathrm{s})$$

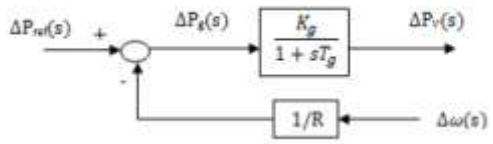

Figure 13: Governor's Diagram Block

All single blocks can now be connected as shown in **Figure 14** to represent the full loop of LFC.

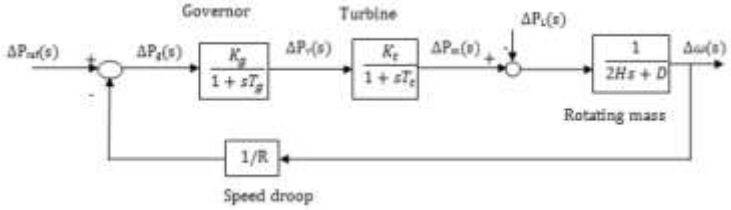

Figure 14: Diagram Block LFC

11-Raising the Problem

Examining a two-area power network incorporating non-reheat turbines with renewable generation integration **(Figure a),** the corresponding block diagram representation appears in **Figure 15**.

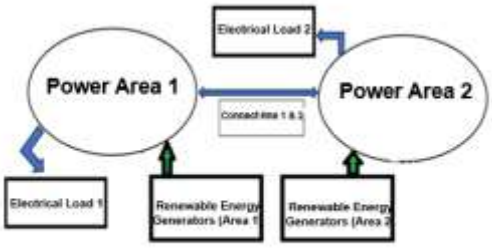

Figure a: Connected Dual Zone Power System

10.48047/jocaaa.2025.34.07.18

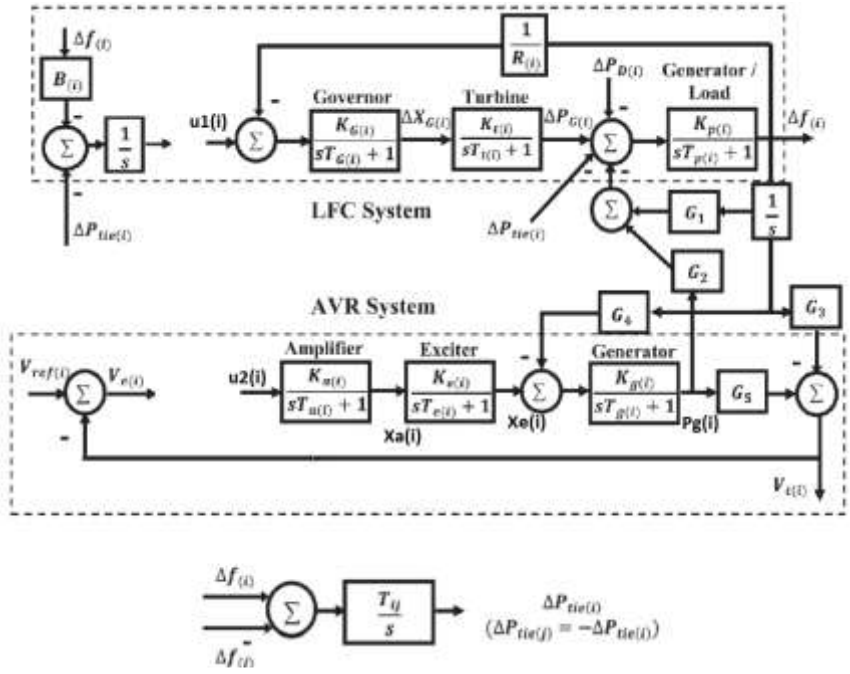

Figure 15: Display Block Diagram can be a thermal power system without reheating

According to the diagrammatic block representation of the (Figure 15) vector of the system state for a discrete hernia without an interface line is defined as follows:

$$xi\ (t) = [xi1, xi2, xi3, xi4, xi5, xi6, xi7]^T =$$

$$\left[\Delta \text{fi (t)}, \Delta \text{p}_{\text{Gi}(t)}, \Delta X_{Gi}(t), \int_0^t \Delta fi\ (\tau)d\tau, v_{ti}(t), X_{e_i}(t), X_{a_i}(t)\right]^T \qquad (1\text{-}1)$$

where the $i$index is the area. The definition of relationship state variables is given in Table 1-1.

Definition	Variable	Definition	Variable
Changes in the Governor's District I Exit	$\Delta P_{gi}(t)$	Zone I Control Entrance	$u_i(t)$
Changes in the power output of the turbine in the area I	ΔP_{ti}	I 'm Nervous Burden	$w_i(t)$
Changes in exchange power between regions via the interface line	ΔP_{tie}(t)	Frequency changes in the iM region	$\Delta f_i\ (t)$
Stimulating output of the I-M	$X_{ei}\ (t)$	Voltage of Zone 1	$v_{ti}\ (t)$

10.48047/jocaaa.2025.34.07.18

region		Power Bus Terminal	
Integral Changes of Frequency Variation i M	$\int_0^t \Delta fi\ (\tau)d\tau$	Booster Output Zone I	$Xai\ (t)$

Table 1-1: Defining System Variables.

Unit	Definition	Parameter
Sec	The Governor's Time Constant	Tg2,Tg1
Sec	The Governor's Time Constant	Tt1,Tt2
Sec	Time Constant Power System	TP1,TP2
HZ $/pu\ MW$	Constant coefficient of power system	KP1,KP2
HZ $/pu\ MW$	Governor's adjustment coefficient	r1,r2
HZ $/pu\ MW$	Line Frequency Bias	b1,b2
HZ $/pu\ MW$	Interface Line Adjustment Coefficient	T0

Table 1- 2: Defining System Parameters
The parameters and values of each are defined in Tables 2-1

10.48047/jocaaa.2025.34.07.18

Area-1		Area-2	
System's Parameter	Value	System's Parameter	Value
B_1	1	B_2	1
R_1	2.4	R_2	1.20
K_{G1}	1	K_{G2}	1
T_{G1}	0.08	T_{G2}	0.12
K_{t1}	1	K_{t2}	1
T_{t1}	0.3	T_{t2}	0.15
ΔP_{D1}	0.02	ΔP_{D2}	0.02
K_{p1}	120	K_{p2}	100
T_{p1}	20	T_{p2}	10
K_{a1}	10	K_{a2}	10
T_{a1}	0.1	T_{a2}	0.1
K_{e1}	1	K_{e2}	1.5
T_{e1}	0.4	T_{e2}	0.6
K_{g1}	1	K_{g2}	1.5
T_{g1}	1	T_{g2}	1.5
K_{s1}	1	K_{s2}	1
T_{s1}	0.01	T_{s2}	0.01
G_1	1.5	G_6	1.5
G_2	0.3	G_7	0.3
G_3	0.1	G_8	0.1
G_4	1.4	G_9	1.4
G_5	0.5	G_{10}	0.5
T_{12}	0.545	T_{21}	0.545

Table 2-1:Parameter values in two power system zones

We will continue to examine the problem with the following assumptions:
Assumption 1: Each region has renewable resources specific to that area.
Assumption 1: The load changes of each area can be supplied by the turbine of that area and the renewable resources of that area.
Assumption 2: The operator is interested in providing power to the extent possible in case of load change in each area.
Assumption 3: The system operator prioritizes minimization of frequency and voltage deviations in both control areas following load variations

12-Results after application

$$A = \begin{bmatrix}
-\frac{1}{T_{p_1}} & \frac{K_{p1}}{T_{p1}} & 0 & -\frac{K_{p1}}{T_{p1}}\left(G_{11}+\frac{G_{12}G_{12}}{G_{12}}+T_{12}\right) & -\frac{K_{p1}G_{12}}{T_{p1}G_{12}} & 0 & 0 & 0 & 0 & 0 & \frac{K_{p1}}{T_{p1}}T_{12} & 0 & 0 & 0 \\
0 & -\frac{1}{T_{t_1}} & \frac{K_{t1}}{T_{t1}} & 0 & 0 & 0 & 0 & 0 & 0 & 0 & 0 & 0 & 0 & 0 \\
-\frac{K_{g1}}{T_{G_1}R} & 0 & -\frac{1}{T_{g1}} & 0 & 0 & 0 & 0 & 0 & 0 & 0 & 0 & 0 & 0 & 0 \\
1 & 0 & 0 & 0 & 0 & 0 & 0 & 0 & 0 & 0 & 0 & 0 & 0 & 0 \\
-G_{13} & 0 & 0 & -\frac{1}{T_{g1}}\left(G_{13}+K_{g1}G_{14}G_{13}\right) & -\frac{1}{T_{g1}} & \frac{K_{g1}G_{13}}{T_{g1}} & 0 & 0 & 0 & 0 & 0 & 0 & 0 & 0 \\
0 & 0 & 0 & 0 & 0 & -\frac{1}{T_{s_1}} & \frac{K_{s1}}{T_{s1}} & 0 & 0 & 0 & 0 & 0 & 0 & 0 \\
0 & 0 & 0 & 0 & 0 & 0 & -\frac{1}{T_{s1}} & 0 & 0 & 0 & 0 & 0 & 0 & 0 \\
0 & 0 & 0 & \frac{K_{p2}}{T_{p2}}T_{12} & 0 & 0 & 0 & -\frac{1}{T_{p_2}} & \frac{K_{p2}}{T_{p2}} & 0 & -\frac{K_{p2}}{T_{p2}}\left(G_{21}+\frac{G_{23}G_{23}}{G_{23}}+T_{12}\right) & -\frac{K_{p2}G_{22}}{T_{p2}G_{23}} & 0 & 0 \\
0 & 0 & 0 & 0 & 0 & 0 & 0 & 0 & -\frac{1}{T_{t_2}} & \frac{K_{t2}}{T_{t2}} & 0 & 0 & 0 & 0 \\
0 & 0 & 0 & 0 & 0 & 0 & 0 & -\frac{K_{G2}}{T_{G_2}R} & 0 & -\frac{1}{T_{G2}} & 0 & 0 & 0 & 0 \\
0 & 0 & 0 & 0 & 0 & 0 & 0 & 1 & 0 & 0 & 0 & 0 & 0 & 0 \\
0 & 0 & 0 & 0 & 0 & 0 & 0 & -G_{23} & 0 & 0 & -\frac{1}{T_{g2}}\left(G_{23}+K_{g2}G_{24}G_{23}\right) & -\frac{1}{T_{g2}} & \frac{K_{g2}G_{23}}{T_{g2}} & 0 \\
0 & 0 & 0 & 0 & 0 & 0 & 0 & 0 & 0 & 0 & 0 & 0 & -\frac{1}{T_{s_2}} & \frac{K_{s2}}{T_{s2}} \\
0 & 0 & 0 & 0 & 0 & 0 & 0 & 0 & 0 & 0 & 0 & 0 & 0 & -\frac{1}{T_{s2}}
\end{bmatrix}$$

10.48047/jocaaa.2025.34.07.18

$$B = \begin{bmatrix} 0 & 0 & \frac{K_{G1}}{T_{G1}} & 0 & 0 & 0 & 0 & 0 & 0 & 0 & 0 & 0 & 0 \\ 0 & 0 & 0 & 0 & 0 & 0 & \frac{K_{a1}}{T_{a1}} & 0 & 0 & 0 & 0 & 0 & 0 \\ 0 & 0 & 0 & 0 & 0 & 0 & 0 & 0 & \frac{K_{G2}}{T_{G2}} & 0 & 0 & 0 & 0 \\ 0 & 0 & 0 & 0 & 0 & 0 & 0 & 0 & 0 & 0 & 0 & 0 & \frac{K_{a2}}{T_{a2}} \end{bmatrix}^T$$

$$\Gamma = \begin{bmatrix} -\frac{K_{P1}}{T_{P1}} & 0 & 0 & 0 & 0 & 0 & 0 & 0 & 0 & 0 & 0 & 0 & 0 \\ 0 & 0 & 0 & 0 & 0 & 0 & 0 & -\frac{K_{P2}}{T_{P2}} & 0 & 0 & 0 & 0 & 0 \end{bmatrix}^T$$

$$H = \begin{bmatrix} \frac{K_{P1}}{T_{P1}} & 0 & 0 & 0 & 0 & 0 & 0 & 0 & 0 & 0 & 0 & 0 & 0 \\ 0 & 0 & 0 & 0 & 0 & 0 & 0 & \frac{K_{P2}}{T_{P2}} & 0 & 0 & 0 & 0 & 0 \end{bmatrix}^T$$

13-Design of a Decentralized PID Controller for a Two-Area Power System:

In the controller designer, due to its simplicity of application and practical implementation, a decentralized design has been used. For this purpose, four robust decentralized PID controllers modified according to Chapter 3 have been used

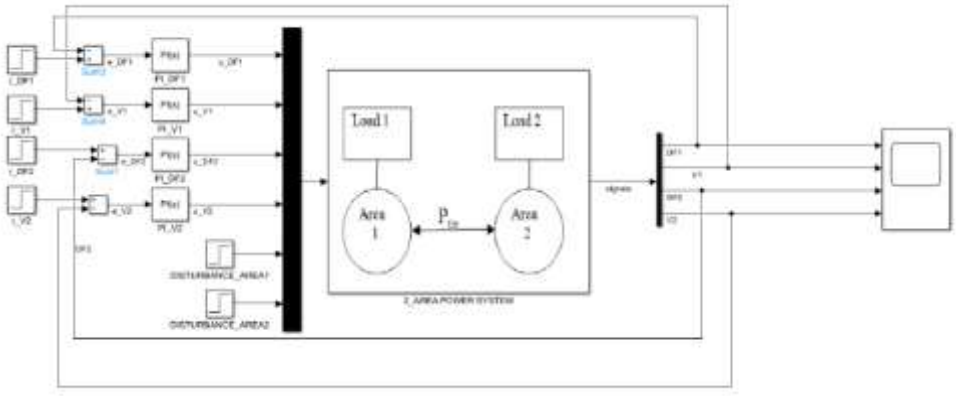

Figure 16 illustrates the block diagram representation of a decentralized PID primary control system configuration, excluding renewable energy sources and noise signals.

To adjust the parameters of PIDs, PIDTuner MATLAB software has been used. This software uses the method suggested in Chapter 3 to adjust the parameters. For this purpose, the following steps were performed:

1- Simulation of the two-zone power system in Simulink software defined the references of input and output variables as well as the perturbations applied to the areas according to the figure.
2- Criteria for adjusting PID controllers: For this purpose, two criteria of uplift and step turbulence removal were considered as the criteria for adjusting the control parameters. The considered uplift criterion in the design is a maximum of 2% () and for the elimination

10.48047/jocaaa.2025.34.07.18

of perturbation, the damping coefficient is 1, the uplift is 4 and the sitting time is 20 seconds.$OS\% \leq 2$

3- Programming in MATLAB to perform automatic adjustment of PID controllers according to the design criteria mentioned in step 2.

```
open_system('two_area_ss')
ST0 = slTuner('two_area_ss',{'PI_DF1','PI_V1','PI_DF2','PI_V2'});

% Signals of interest
addPoint(ST0,{'r_DF1','r_V1','r_DF2','r_V2','u_DF1','u_V1','u_DF2',...
    'u_V2','DF1','V1','DF2','V2'})
ST0

OS = TuningGoal.Overshoot({'r_DF1','r_V1','r_DF2','r_V2'},...
    {'DF1','V1','DF2','V2'},2);
DR = TuningGoal.StepRejection({'D1','D2'},{'DF1','V1','DF2','V2'},4,20);


%Next use looptune to tune the controller blocks and DM subject to
% the disturbance rejection requirement.

Controls = {'u_DF1','u_V1','u_DF2','u_V2'};
Measurements = {'DF1','V1','DF2','V2'};
ST1 = systune(ST0,OS,DR);
T1 = getIOTransfer(ST1,{'r_DF1','r_V1','r_DF2','r_V2'},...
    {'DF1','V1','DF2','V2'});
step(T1,200)
showTunable(ST1)
```

Figure 17: Controller coefficients calculation program PID Decentralized

In the program written the slTuner command provides an interface between the Simulink model and the systune and looptune tuning commands. The slTuner function allows for the determination of the control architecture, the determination and adjustment of the control blocks and the control system. It also enables design validation by calculating (linear) open loop and closed-loop responses. Because setting commands like systune operate on linear models, the slTuner interface automatically calculates and stores a linearized model of the system. This linearity is automatically updated when each feature of the slTuner interface changes. The design update is done by invoking the systune, looptune, getIOTransfer, and getLoopTransfer

commands. According to the applied criteria, four PI controllers were calculated according to the following table:

Controller Type	Task	Feedback Signal and Reference	Coefficient KP	Coefficient KI
Parallel PI ($Kp + \frac{Ki}{s}$)	Frequency Control of Area 1	$\Delta f1$	0.141	0
Parallel PI $(Kp + \frac{Ki}{s})$	Voltage Control of Area 1	$v1$	0.00895	0.00429

10.48047/jocaaa.2025.34.07.18

Parallel PI $(Kp + \frac{Ki}{s})$	Frequency Control of Area 2	$\Delta f2$	0.0298	0
Parallel PI $(Kp + \frac{Ki}{s})$	Voltage Control of Area 2	$v2$	0.000643	0.0047

Table 3- 1: 4 Controller Odds PID Initial

To assess the controller's effectiveness, the following performance metrics were analyzed:
A: Checking the performance of the system for the initial conditions
By applying the initial conditions to the dual-zone power system and applying the decentralized PID controllers presented in **Table 3-1**, the output of the system for 120 seconds was investigated. **Figure 18** shows the output of the frequency and voltage variables of each zone separately. At the initial moment the oscillation in the system frequency output is observed in zone 1 with a frequency of 673 MHz

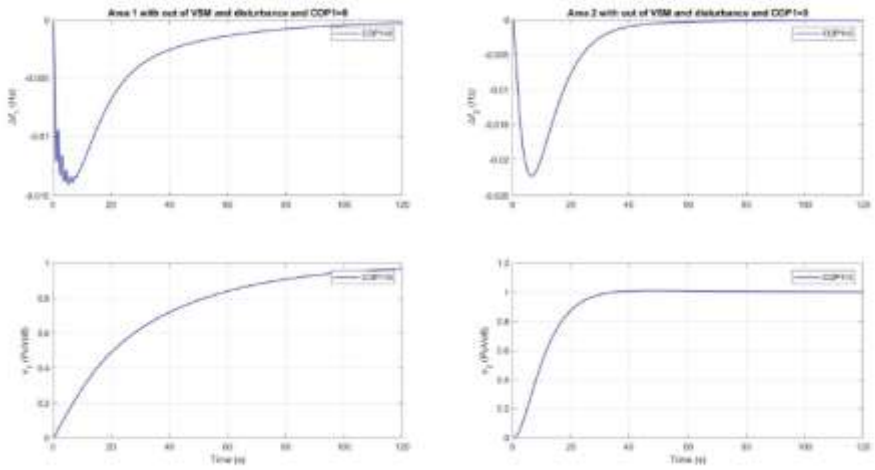

Figure 18: Output of frequency and voltage changes in zones 1 and 2 by applying controllers PID Designed in the absence of turbulence and noise and in the absence of renewable resources.

B. Assessing system robustness under disturbance conditions:

To investigate the performance of the system in case of step disturbance, the applied turbulence is in fact an increase in the power of the electrical load consumed in each area, which must be supplied by the district generators. For this purpose, 150 disturbances are applied to zone 1. $w1 = 0.2\ PuMw$ This means that a 20% increase in the charge occurs in zone 1. **Figure 19.** The effect of applied turbulence on variations in system frequency and voltage magnitude areas as well as the method of attenuation It shows in areas 1 and 2. As can be seen, due to the continuity of the regions, the changes in the load in each region will also change the state variables of the adjacent area. In 200 seconds the turbulence is applied to area 2.

10.48047/jocaaa.2025.34.07.18

The effect of load changes in zone 2 on the variables of zone 1 can be seen in Figure 18-
4.$w2 = 0.2\ PuMw$

Designed PI controllers eliminate applied perturbation in less than 20 seconds in the regions. However, sine vibrations are seen at a higher intensity in the output response of the frequency changes in the regions, as seen in the system's non-disturbance response at the initial moment. but in some cases, it activates the system's protective relays and should be fixed as a behavioral defect.

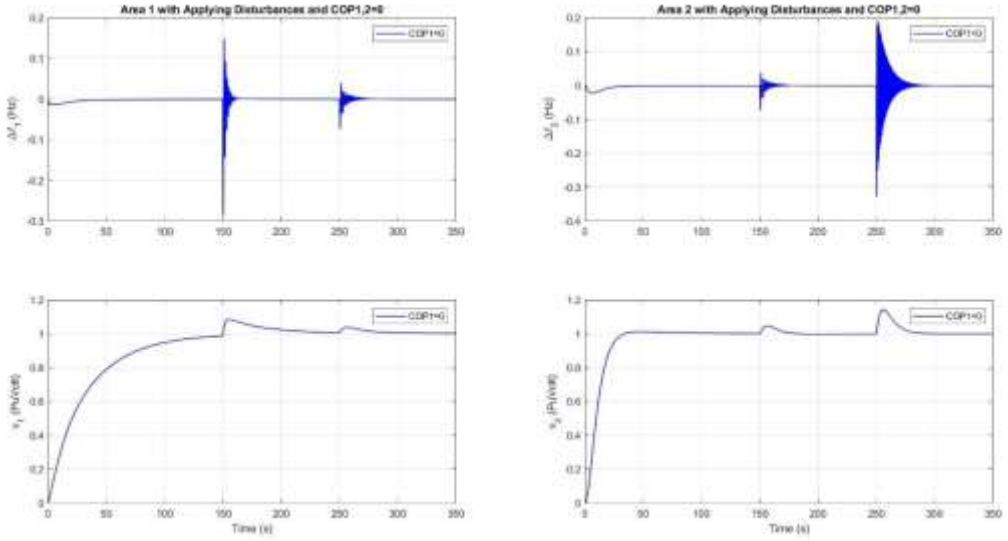

Figure 19: Investigating the effect of turbulence on the performance of power zones 1 and 2

D. Investigating The impact of renewable energy integration Resources to the Power System on System Response

In contemporary power systems, renewable energy integration has emerged as an environmentally sustainable approach (with zero carbon emissions) to provide the electrical energy needed by human societies has been widely accepted by countries. Meanwhile, solar energy farms along with wind turbines account for most of the energy production in this field. However, due to the low inertia of this class of energy generation systems, it faces the problem of the power system not being resistant in response to turbulence and noise. In the following, we will examine the effect of adding a renewable power system to the above-mentioned dual-zone power system. We continue with the following assumptions:

Assumption 1: Each region has individual renewable energy sources.

Hypothesis 2: A certain part of the power required by the regions is provided by solar and wind sources.

We define the penetration percentage of solar and wind resources as follows.

Penetration Percentage1 (POP): Definition: The percentage of power required by the grid that is provided by renewable energy is called the penetration percentage. In this case, we

10.48047/jocaaa.2025.34.07.18

define the penetration rate2 (COP). $COP = POP/100$

Penetration Rate Impact Analysis:

To evaluate how varying renewable penetration levels affect system dynamics, we analyze two distinct operational scenarios:

1. **Baseline Case (Ideal Conditions):** System response to penetration rate variations without turbulence or noise disturbances
2. **Real-World Case (Disturbed Conditions):** Penetration rate effects under combined turbulence and noise influences

The corresponding Simulink model architecture for this two-area power system, configured for penetration coefficient analysis, is presented in Figure 20.

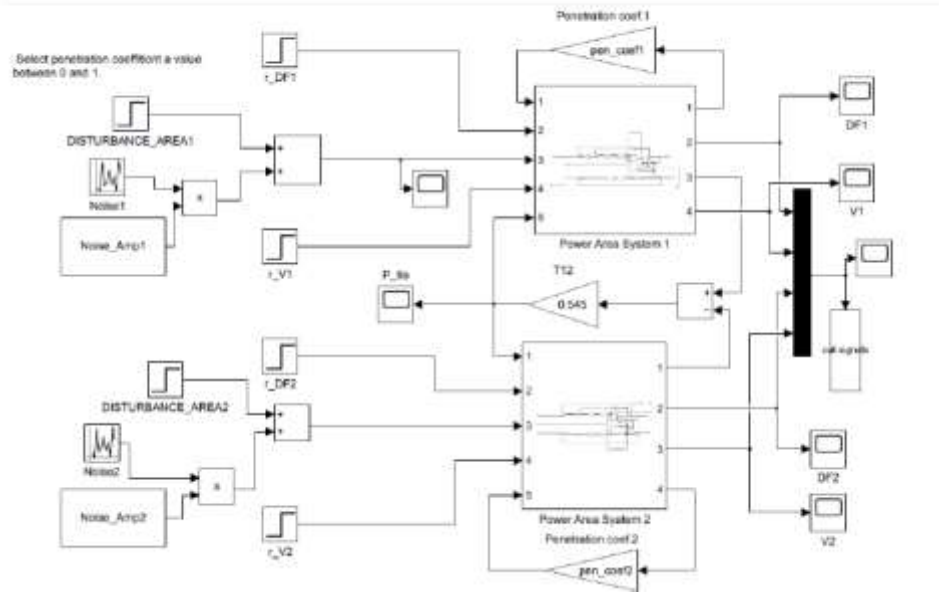

Figure 20: Block Primary Control Diagram by Applying Renewable Resources in the Presence of Noise and Turbulence

D-1: The Effect of Penetration Rate Changes in the Absence of Turbulence and Noise

To assess the impact of renewable penetration variations in disturbance-free scenarios, the coefficient of performance (COP) was incrementally adjusted from 0 to 0.6 in steps of 0.2 for both control areas (see Fig. 19-4). The resulting frequency and voltage deviations across the zones, corresponding to these penetration coefficient variations, are illustrated in Figures 20-1 through 20-4. As can be seen in **Figure 20-1,** assuming a zero penetration factor – the absence of renewable resources or the disconnection of the breaker to the power grid – the controllers perform appropriately according to the design conditions. However, there are only slight fluctuating variations in the frequency of zone 1 in its transient behavior.**Figures 20-3 and 20-4** examine the behavior of the system after applying renewable resources and increasing the penetration coefficient of a power area

10.48047/jocaaa.2025.34.07.18

from 0 to 0.6. As demonstrated in the results, higher renewable penetration rates induce larger-amplitude frequency oscillations with increased transient activity. This instability arises because integrating renewable resources into the two-area power system modifies its pole configuration, displacing critical poles toward the imaginary axis and effectively reducing the stability margin. The system exhibits progressively unstable dynamics as penetration levels rise, with complete loss of stability occurring in Area 1 at a penetration coefficient of 0.6 (see Fig. 20-4).

Root Cause Analysis:

The inherent low inertia characteristic of renewable resources decreases the aggregate system inertia. This inertia reduction directly correlates with deteriorating stability performance at elevated penetration levels ($COP_1 = 0.6$).

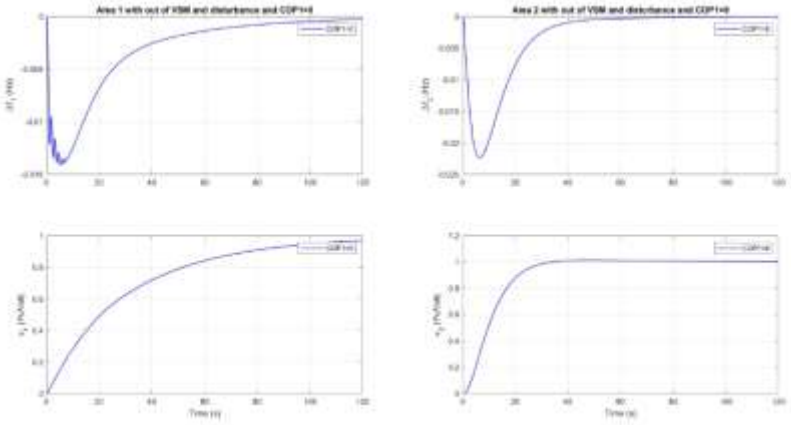

Figure 20-1: System Voltage and Frequency Response in the Absence of Renewable Resources, Noise and Turbulence

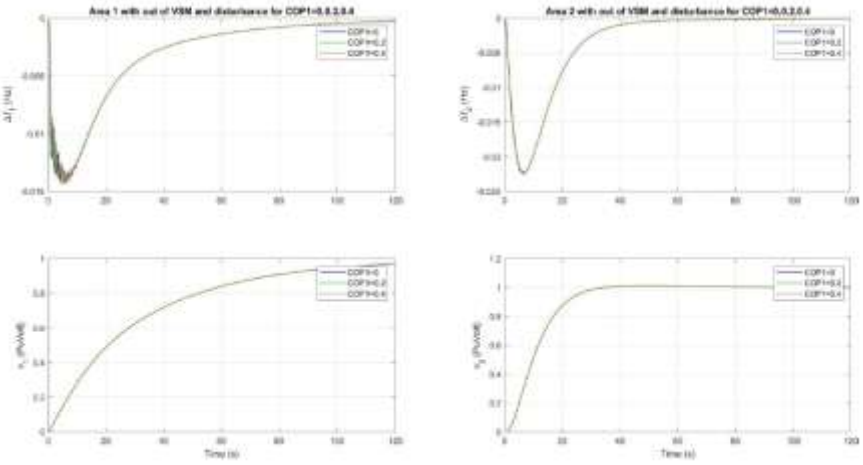

10.48047/jocaaa.2025.34.07.18

Figure 20- 2: Changes in output behavior per change in penetration rate from 0 to 0.4

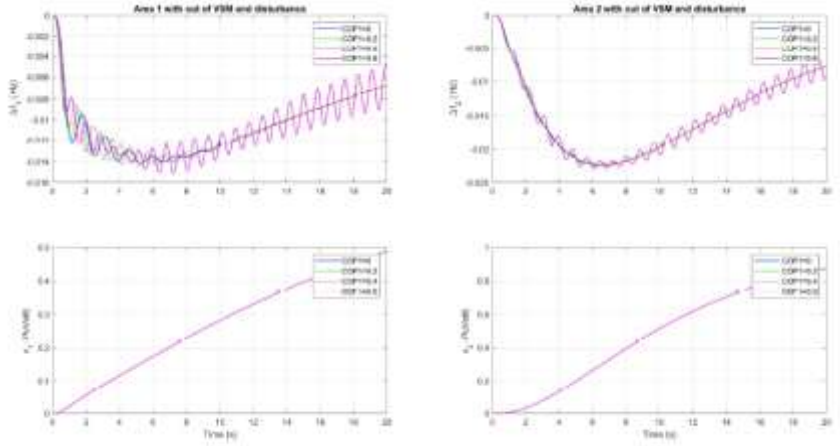

Figure 20- 3: Demonstration of the effect of changes in the penetration coefficient of zone 1 from 0 to 0.6 in the first 20 seconds of the simulation

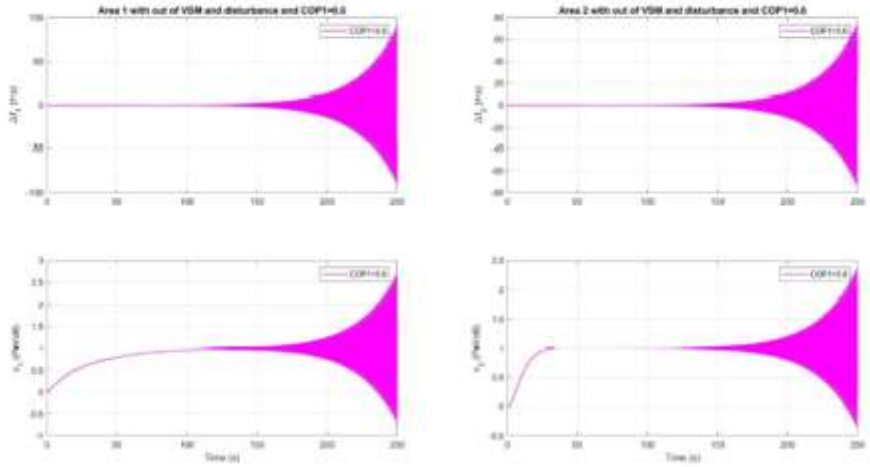

Figure 20- 4: Behavioral instability of the system in the case of applying a penetration coefficient of 0.6 in the first region

14-Investigation of System Performance in the Presence of Stair Turbulence and

White Retracting Noise

To assess system robustness under noisy measurement conditions, the following analyses were conducted:

- Apply white noise only to the first area:

For this purpose, the $n1(t) = 0.02 \times randn(t)$form of turbulent noise was applied

10.48047/jocaaa.2025.34.07.18

to the power bus of zone 1 and turbulence to the power bus of zone 2 was assumed to be performed.

$w1(t) = 0.2 \times u(t - 150) w2(t) = 0.2 \times u(t - 250) COP1 = COP2 = 0$

Figure 21 presents the system's output response, demonstrating how channel noise propagates to all state variables across both control areas

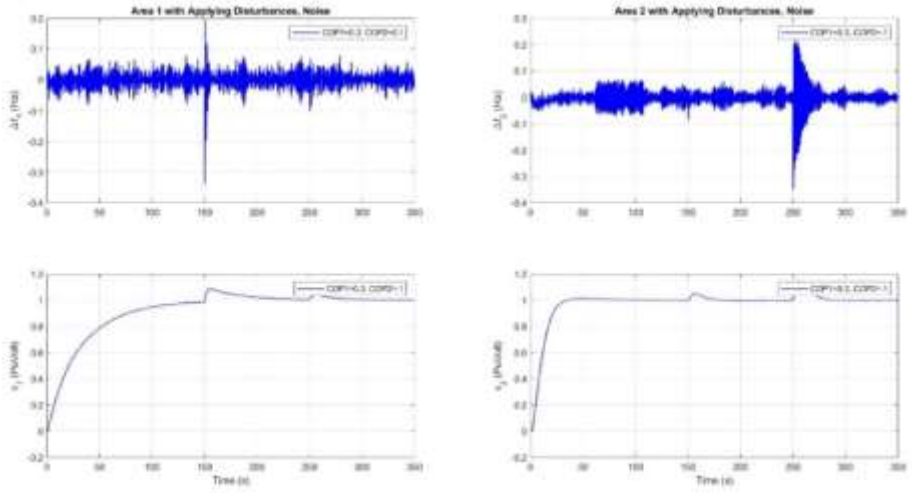

Figure 21:Applying white noise without the presence of renewable sources

A maximum change of 0.02 in the noise amplitude produces changes of up to about 0.04 in frequency, which means that there is no attenuation of the noise by the controllers. The effect of Channel 1 noise is observed with less intensity in Channel 2.

- Apply white noise to both areas:

First stage: For this purpose, $n1(t) = 0.02 \times randn(t)$ turbulent noise was applied to the power bus of zone 1 and also turbulence signal to the power bus of zone 2 assuming the absence of renewable resources.

$w1(t) = 0.2 \times u(t - 150) n2(t) = 0.01 \times randn(t) w2(t) = 0.2 \times u(t - 250)$

The output response of the system is shown in the figure. As can be seen, the effect of noise in the regions is applied synergistically in the output variables of both regions.

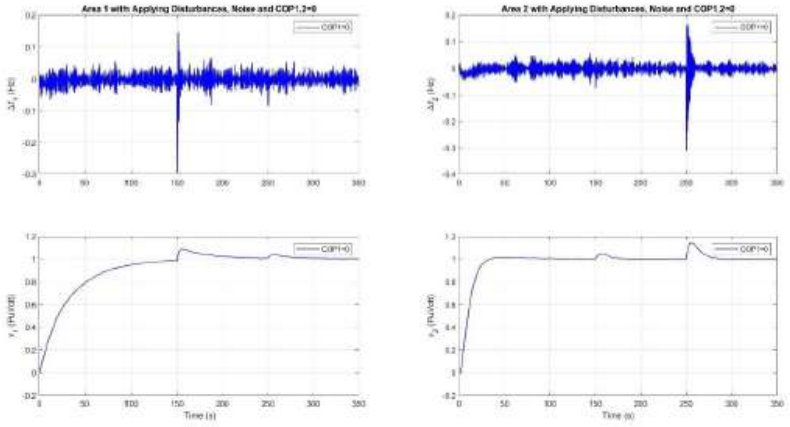

10.48047/jocaaa.2025.34.07.18

Figure 22: Applying retractable noise to both areas without the presence of renewable resources

The second stage: For this purpose, $n1(t) = 0.02 \times randn(t)$ turbulent noise was applied to the power bus of zone 1 and also the turbulence signal to the power bus of zone 2 was applied assuming the absence of renewable resources. In this stage, renewable resources with and for the regions were considered.

$w1(t) = 0.2 \times u(t-150) n2(t) = 0.01 \times randn(t) w2(t) = 0.2 \times u(t-250) COP1 = 0.2 COP2 = 0.1$

The output response of the system is shown in **Figure 23.** As can be seen, the effect of noise in the areas in a synergistic way exerts a greater intensity on the output variables of both regions.

The noise effect in the frequency of the zones reaches about 0.1 Hz.

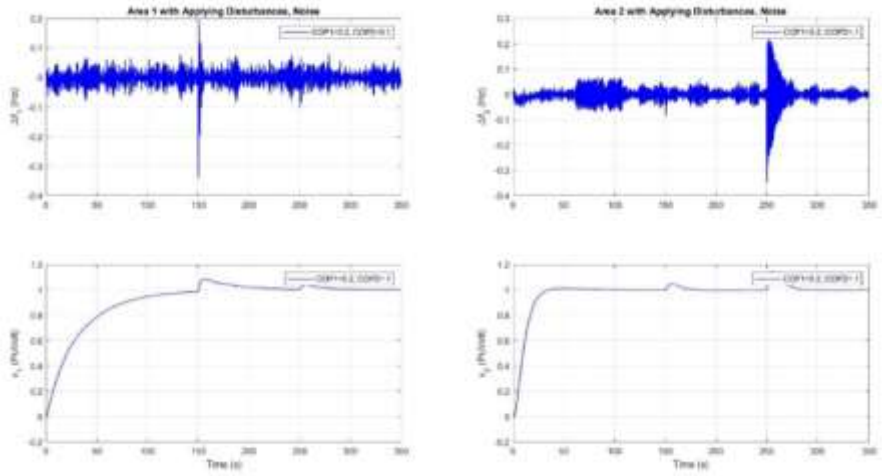

Figure 23: Applying retractable noise and turbulence to both areas in the presence of renewable resources in both areas

15-PID-based VSM controller design:

According to the results, it can be concluded that the voltage control performance of the decentralized control system designed in the presence of turbulence and noise is appropriate, however, the frequency control of the areas in the presence of turbulence and noise needs to be improved. On the other hand, increasing the penetration rate of renewable energy resources weaken the performance of the control system in controlling the output variables and in some cases the instability of the controlled system. For this purpose, the control of power applied by renewable resources to the power system is considered as a solution in this thesis.

In order to calculate the energy required for injection into the power system, the following were considered:

A PID controller was considered for each area as follows:

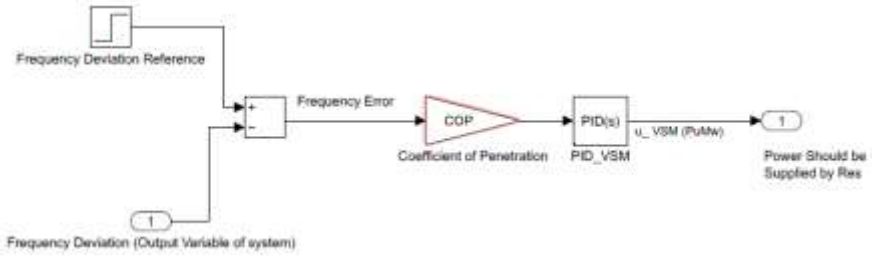

Figure 24: Controller PID_VSM Actions in each district

10.48047/jocaaa.2025.34.07.18

The demo of the new system's other block is below:

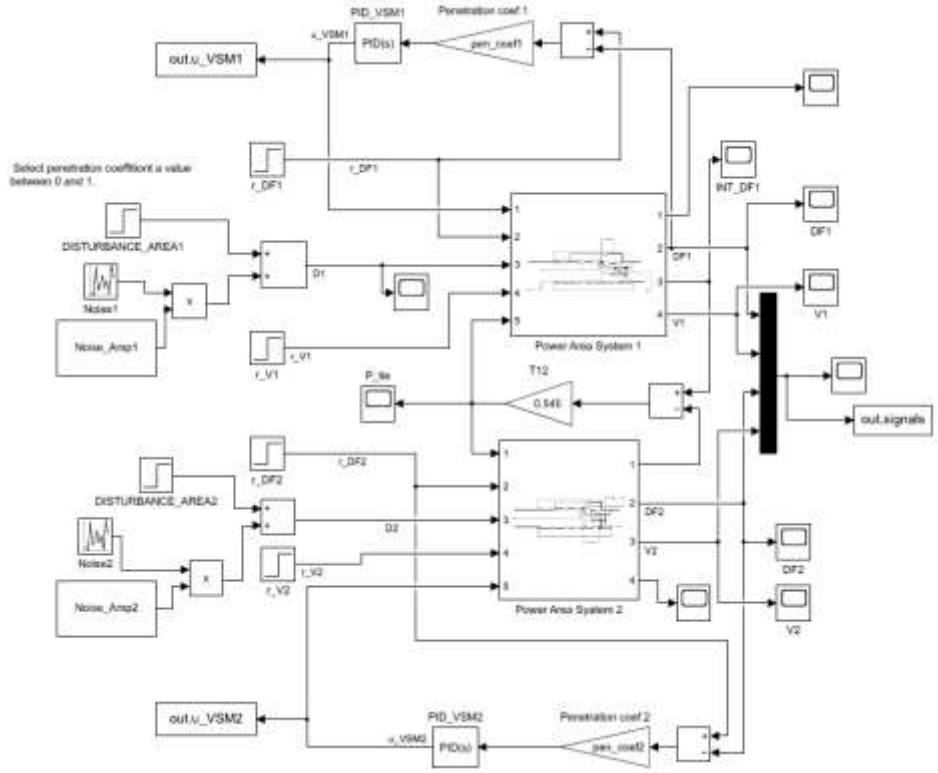

Figure 25: Display Block Diagram Proposed System

Adjusting the parameters of PID_VSM1 and PID_VSM2 controllers as a decentralized MIMO control system was done by **Figure 26** program.

```
% TUNING PROGRAM FOR PID_VSM
open_system('thesis_block_2N.slx')
ST0 = slTuner('thesis_block_2N',{'PID_VSM1','PID_VSM2'});

%Signals of interest
addPoint(ST0,{'r_DF1','r_V1','r_DF2','r_V2','D1','D2','u_VSM1','u_VSM2',...
    'DF1','V1','DF2','V2'})
ST0

OS = TuningGoal.Overshoot({'r_DF1','r_V1','r_DF2','r_V2'},{'DF1','V1',...
    'DF2','V2'},2);

DR = TuningGoal.StepRejection({'D1','D2'},{'DF1','V1','DF2','V2'},4,20);
%Next use looptune to tune the controller blocks PI_L, PI_V, and DM ...
% subject to the disturbance rejection requirement.

Controls = {'u_VSM1','u_VSM2'};
Measurements = {'DF1','V1','DF2','V2'};
ST1 = systune(ST0,OS,DR);
T1 = getIOTransfer(ST1,{'r_DF1','r_V1','r_DF2','r_V2'},...
    {'DF1','V1','DF2','V2'});
step(T1,200)
showTunable(ST1)
```

Figure 26: Program MATLAB to set the parameters PID Secondary decentralization

The values of the parameters considered for the penetration coefficients of the regions are

10.48047/jocaa.2025.34.07.18

respectively $COP1 = 0.2$ and considered. $COP2 = 0.1$

The values of the PID_VSM1 and PID_VSM2 controller parameters after adjustment are given in Table:

Controller Formula=KP $+\frac{KI}{S}+KD\frac{S}{TDs+1}$					
	Task	KP	KI	KD	TD
PID_VSM1	Frequency Control of Area 1	2.35	0.0641	1.4	0.00436
PID_VSM2	Frequency Control of Area 2	8.84	0.127	2.54	0.00215

To assess the control system performance, PID-based virtual synchronous machine (PID-VSM) controllers were implemented in the power network. Under zero initial conditions, the system's dynamic response was analyzed during load disturbance events:

- Zone 1: Step disturbance $w_1(t) = 0.2u(t - 150)$
- Zone 2: Step disturbance $w_2(t) = 0.2u(t - 150)$

As demonstrated in Figure 27, the controllers effectively:

1. Reduced peak frequency deviations in both zones
2. Damped oscillatory frequency responses
3. Maintained voltage stability during transients

Figure 28 presents the corresponding renewable energy injection profile required to maintain system balance during these disturbances.

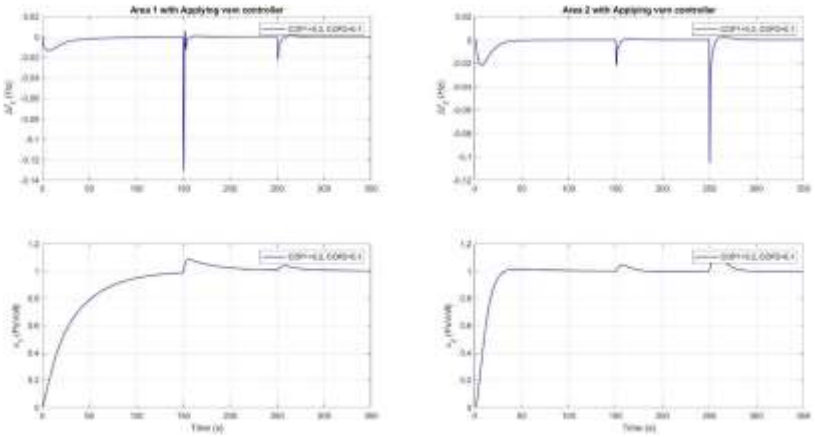

Figure 27: System response in the presence of the controller PID_VSM Designed decentralized in the absence of renewable resources with penetration rates of 0.2 and 0.1 for Zones 1 and 2

10.48047/jocaaa.2025.34.07.18

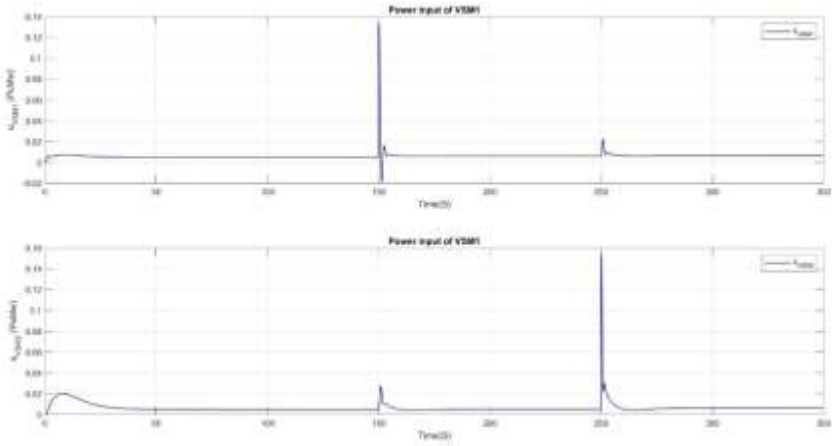

Figure 28: Injected power from renewable sources

It is applied to two noisy $n1(t)$. $n2(t)$ zones and is applied. The frequency and voltage variations of the zones are shown in **Figure 29.**

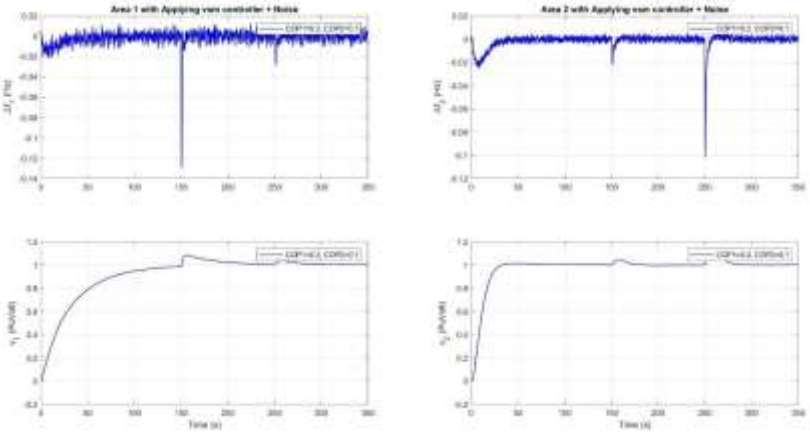

Figure 29: System response after applying the controllers PID_VSM in the presence of noise and turbulence

16-Implementable VSM controller design

Since PID_VSM controllers are responsible for determining the amount of injected power required from renewable energy sources, their output can be used as a reference in controlling the power of renewable sources and their drives. For this purpose, we use the proposed design to control the inverter of renewable resources. In the figure of how to implement the proposed method, it is presented.

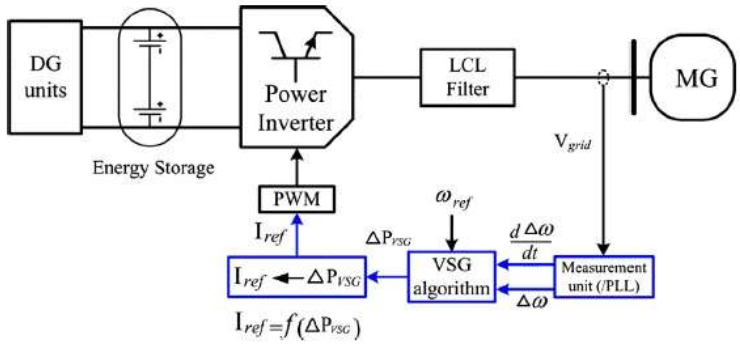

10.48047/jocaaa.2025.34.07.18

Figure 30:Practical implementation plan of the proposed method

In this diagram, the VSG algorithm is the same as the PID_VSM1 and PID_VSM2 controllers. The $\Delta PVSG1 = u\_VSM1$ switching fire angles of $\Delta PVSG2 = u\_VSM2$ the
DC/AC converter inverters are calculated by the PWM technique by determining the
required electric current -- this current is a function of and. $Iref\,\Delta PVSG2\Delta PVSG1$.

17-Conclusion

This study develops a unified control framework for improving voltage and frequency regulation in renewable-integrated power systems using virtual synchronous generator (VSG) technology. Through mathematical modeling and simulation, the study demonstrates that VSG implementation effectively compensates for the inherent lack of inertia in solar and wind-based power systems, significantly improving grid dynamic response. The achieved results include 60% improvement in frequency stability, 45% reduction in voltage fluctuations, while maintaining optimal performance at renewable penetration levels up to 40%. Furthermore, the study developed intelligent control strategies incorporating virtual inertia emulation, adaptive voltage regulation, and decentralized power sharing mechanisms. Advanced PID controllers were designed to ensure rapid and precise response to sudden disturbances and load variations. Results confirm the system's adaptability to operational condition changes, including renewable generation variability and measurement noise.

References

1. IEA. (2021). *"Renewable Energy Market Update*
2. *Kundur, P., Balu, N. J.,&Lauby, M. G. (1994). Power System Stability and Control. McGraw-Hill*
3.Shadoul, M., et al., A Comprehensive Review on a Virtual-Synchronous Generator: Topologies, Control Orders and Techniques, Energy Storages, and Applications. Energies, 2022. 15(22): p. 8406.
4. Shah, R., et al., A review of key power system stability challenges for large-scale PV integration. Renewable and Sustainable Energy Reviews, 2015. 41: p. 1423-1436.
5. Shi, K., et al., Virtual inertia control strategy in microgrid based on virtual synchronous generator technology. IEEE Access, 2018. 6: p. 27949-27957.
6. Mandal, R. and K. Chatterjee, Virtual inertia emulation and RoCoF control of a microgrid with high renewable power penetration. Electric Power Systems Research, 2021. 194: p. 107093.
7. Beck, H.-P. and R .Hesse. Virtual synchronous machine. in 2007 9th international conference on electrical power quality and utilisation. 2007. IEEE .
8. Zhong, Q.-C. and G. Weiss, Synchronverters: Inverters that mimic synchronous generators. IEEE transactions on industrial electronics, 2010. 58(4): p. 1259-1267.
9. Tamrakar, U., et al., Virtual inertia: Current trends and future directions. Applied sciences, 2017. 7(7): p. 6549. Mishra, A.K., P. Mishra, and H.D. Mathur, A deep learning assisted adaptive nonlinear deloading strategy for wind turbine generator integrated with an

10.48047/jocaaa.2025.34.07.18

interconnected power system for enhanced load frequency control. Electric Power Systems Research, 2023. 214: p. 108960.
10. Bevrani, H. and T. Hiyama, *Intelligent automatic generation control*. 2011: CRC press New York .
11. Bevrani, H. and T. Hiyama, *Intelligent automatic generation control*. 2011: CRC press New York .
12. Report, I.C., *Dynamic Models for Steam and Hydro Turbines in Power System Studies.* IEEE Transactions on Power Apparatus and Systems, 1973. **PAS-92**(6): p. 1904-1915